LAWRENCE
LIVERMORE
NATIONAL
LABORATORY

LLNL-JRNL-675169

Analysis of the neutron time-of-flight spectra from inertial confinement fusion experiments

R. Hatarik, D. B. Sayre, J. A. Caggiano, T. Phillips, M. J. Eckart, G. P. Grim, E. P. Hartouni, J. M. Mcnaney, D. H. Munro

July 24, 2015

Journal of Applied Physics

Disclaimer

Analysis of the neutron time-of-flight spectra from inertial confinement fusion experiments

R. Hatarik,[1, a)] D. B. Sayre,[1] J. A. Caggiano,[1] T. Phillips,[1] M. J. Eckart,[1] G. P. Grim,[1] E. P. Hartouni,[1] J. M. Mcnaney,[1] and D. H. Munro[1]
Lawrence Livermore National Laboratory

(Dated: 23 July 2015)

Neutron time-of-flight (nToF) diagnostics have long been used[1–3] to characterize the neutron spectrum produced by inertial confinement fusion (ICF) experiments. The primary diagnostic goals are to extract the fusion neutron yields, neutron peak widths and the rate of neutron scattering relative to the primary neutron yield, also known as the down-scatter ratio (DSR). These quantities are used to infer burn weighted plasma conditions, such as ion temperature (T_{ion}) and fuel areal density. We report on novel methodologies developed to facilitate the reliable determination of neutron yield, apparent T_{ion} and DSR. These methods invoke a single temperature, static fluid model, to describe the neutron peaks from $d+d \rightarrow n+^3$He (DD) and $d+t \rightarrow n+\alpha$ (DT) reactions and a spline generated description of the spectrum for determining the rate of DT neutron scatters. Both measurements are performed using a forward modeling technique that includes corrections for line-of-site attenuation and detection system impulse response. These methods produce typical uncertainties for DT T_{ion} of 260 eV, 7% for DSR, and 9% for the DT neutron yield. For the DD values the uncertainties are 290 eV for T_{ion} and 10% for the neutron yield.

I. INTRODUCTION

The National Ignition Facility (NIF) delivers up to 2 MJ of 3ω (351 nm) laser light to a hohlraum target containing a spherical capsule, typically filled with deuterium and tritium or deuterium and ^{3}He fuels[4,5], with the goal of imploding that capsule and creating thermonuclear fusion. Measurement of neutron spectral details for all implosions which create measurable neutron yield is a goal of the neutron Time-of-Flight (nToF) diagnostic program.

Previous[1–3] descriptions of nToF data analysis from DT fusion neutrons typically attempted to deconvolve (unfold) the instrument response from the data or used the assumption that the spectrum is a Gaussian convolved with a response of instant rise followed by a sum of exponential decays[3]. We found that deconvolution introduces unphysical artifacts into the data, while the correct interpretation of the nToF signals at NIF requires a more detailed description of the instrument response than a simple model of instant rise with exponential decay can provide.

In order to characterize the neutron spectrum of ICF implosions, we return accurate measures of several characteristic and descriptive quantities. For DT filled capsules these are the primary DT neutron yield near 14 MeV, the DD neutron yield near 2.5 MeV, the spectral width of both peaks, which depend on the ion temperature (T_{ion}) of the plasma, and a scalar measure of the DT down-scattered spectrum around 11 MeV and thus the cold fuel ρR. For DD filled capsules we measure the primary DD neutron yield near 2.5 MeV, and the spectral width of that peak. Additionally for many implosions we extract neutron spectra from about 16 MeV to about 2 MeV, with a dynamic range of about 4 orders of magnitude. This paper will focus on the methods used to analyze nToF data: the models assumed where such assumptions are made, the fitting methods employed, the role of instrument response functions, and the subsequent errors of the measured quantities. The following conventions were chosen: the neutron yield Y_n are the neutrons emitted with an energy range depending on the reaction. For DT the range is from 13 MeV to 15 MeV, for DD it is from 2.2 MeV to 2.7 MeV and for TT it is from 5 MeV to 10 MeV. The down-scattered ratio (DSR) is defined as the neutron yield from 10 MeV to 12 MeV divided by Y_n.

The structure of the paper is as follows: first a brief overview of the nToF data acquisition is given, then the fit of a nToF data model is explained, which includes details on components of the fit like the instrument response function and the sensitivity of the instrument. Finally two different models are presented and example fits on those are shown. Lastly an overview of how the uncertainties of the deduced values was determined is given.

II. DATA ACQUISITION

The above described quantities can be measured with high precision nToF spectrometers. Four nToF detectors are located at about 20 m from the Target Chamber Center (TCC) of NIF to measure the neutron spectrum on their respective lines-of-sight. Those detectors use a fast organic scintillator to detect neutrons and the scintillation light is detected with Photomultiplier Tubes (PMT) and Photodiodes (PD). The detector setups have been described in Refs[6–9]. To measure the yield and ion temperatures from the neutrons associated with the DD fu-

[a)] hatarik1@llnl.gov

sions that take place during DT fusion shots, three of the nToF detectors have higher gain, gated PMTs. To insure the linear response of the photo detectors, the total charge drawn from a photo detector was limited to 5 nC by a combination of timing gates and scintillator light attenuators.

Each PMT/PD signal is recorded on a high bandwidth digital oscilloscope (Tektronix DPO7104), which have 8 bit digitizers ($\approx$ 6 effective bit). To obtain a reliable DSR measurement, it is necessary to combine two channels recorded with different sensitivity together in order to obtain a stitched trace which has higher sensitivity in the down-scattered region of the signal while retaining the unclipped peak of the less sensitive channel. To accomplish this each signal goes through a signal splitter and is recorded with different sensitivity on multiple scope channels. The algorithm that stitches those together works as follows: the two channels to be combined are being identified as the most sensitive channel that does not contain any saturated data point and the next more sensitive channel. The uncertainties of each data point are dominated by the scope noise. They are determined by building average and standard deviation over a part of the spectrum containing only the baseline. The average is subtracted from each data point to set the baseline of the combined trace to zero. Both traces are then scaled so that the their values correspond to the output voltage of the PMT/PD. Next the time difference of both traces is determined such that the χ^2 between the two channels on the rising edge of the main neutron peak is minimized. To allow for sub sample shifts a linear interpolation between data points on the more sensitive channel is used. Finally each data point of the combined trace is calculated as weighted average of both traces, except for the region in which the more sensitive channel is saturated. It has been observed that after a scope trace clips it overestimates the signal for some time and gradually approaches the value of the non saturated trace. Therefore the saturated region of the sensitive scope trace is determined from the first clipped data point until it agrees within one standard deviation to the less sensitive channel.

III. FORWARD FITTING NTOF SPECTRA

Removing the detector response from the nToF data would require a deconvolution, which is mathematically not a well posed problem. Therefore it was chosen to preform a χ^2-fit to the nToF scope signals in time with a function determined by parametrizing the neutron spectrum with a model, taking into account the detector sensitivity and the beam line attenuation, and convolving it with the instrument response function (IRF). The fit function takes the following form:

$$f(t) = I(E(t))s(E(t))a(E(t))\frac{dE}{dt} \otimes R(t) \qquad (1)$$

Here $I(E)$ denotes the model of the neutron spectrum, $s(E)$ is the sensitivity of the detector to the given neutron energy, $a(E)$ is the beam line attenuation factor, $E(t)$ is the neutron energy as a function of time-of-flight, $\frac{dE}{dt}$ converts the energy spectrum into time-of-flight space, $R(t)$ is the instrument response and t_0 is the time offset needed to convert the scope time axis into time-of-flight. $E(t)$ is given by:

$$E(t) = m_n(\gamma - 1),\ \gamma = \left(1 - \beta^2\right)^{-\frac{1}{2}},\ \beta = \frac{t}{t_\gamma} \qquad (2)$$

with t_γ being the time-of-flight of a photon from TCC to the detector (given as distance over speed of light) and m_n the energy of the neutron at rest due to its mass. Then $\frac{dE}{dt}$ is given by:

$$\frac{dE}{dt} = \frac{m_n\gamma^3\beta^3}{t_\gamma} \qquad (3)$$

The determination of the instrument response ($R(t)$), the scintillator sensitivity ($s(E)$) and the beam line attenuation ($a(E)$) are described below. The models used for $I(E)$ in Eqn. (1) and their application in the data analysis are explained in section IV.

A. Instrument response function (IRF)

To determine the neutron spectrum accurately the IRF of the detector has to be known, which is most important in understanding T_{ion} and DSR of the DT neutron spectrum. This is due to the width of the IRF being a sizeable fraction of the DT peak width and the tail of the IRF causes a background in the down-scattered part of the neutron spectrum. Therefore it is important to know the IRF with reasonable precision in order to get low uncertainties for the values of DT T_{ion} and DSR. It is also important to note that due to the asymmetry in the IRF a direct conversion of the raw nToF signal scope time axis into neutron energy is not possible, i.e. the position of the peak on the scope trace depends not only on the position of the peak in the source spectrum, but also on the shape of the source spectrum as well.

The IRF was constructed using the X-ray impulse of a timing shot, which has a FWHM of typically $\approx$100 ps, as an approximation of an impulse response for photons. To obtain a neutron IRF it is necessary to include the time it takes for a neutron to traverse the scintillator. To model this part of the IRF an MCNP simulation that histograms neutron energy deposition in the scintillator over time was done and convolved with the X-ray impulse data. Since DD and DT neutrons take different amounts of time to traverse the scintillator, this had be done separately for DD and DT neutrons creating separate IRFs for each reaction. Fig. 1 shows the obtained IRF for 14 MeV neutrons of the south pole nToF detector.

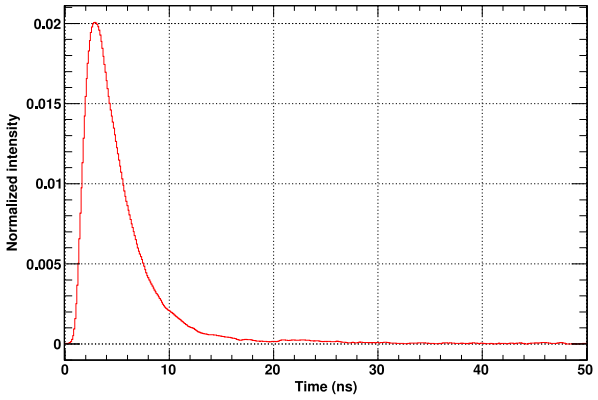

FIG. 1. The IRF of the south pole nToF detector for DT neutrons.

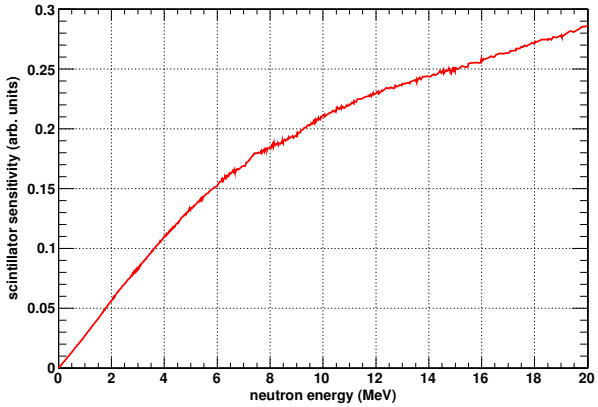

FIG. 2. The sensitivity of the Bibenzyl scintillation crystal as a function of neutron energy.

B. Scintillator sensitivity

The scintillator sensitivity as a function of neutron energy was simulated by a program based on the Stanton[10] code. The code was modified to tabulate light yield instead of efficiency and pulse height distribution. This code uses the Monte Carlo method to track neutrons traversing the scintillator, taking into account the scintillator geometry. It uses the neutron interaction cross sections to determine the charged particles produced and their light output. The reactions included are elastic proton and carbon scattering and inelastic carbon scattering including the reactions $^{12}\mathrm{C}(n,\alpha)^{9}\mathrm{Be}$ and $^{12}\mathrm{C}(n,3\alpha)$. The cross sections for these calculations were taken from the ENDF/B-VI evaluation. In the code scattered neutrons are being tracked for secondary interactions until their energy falls below 0.1 MeV. The light output for each charged particle is determined separately using fits to the data given by Verbinski *et al*[11]. Fig. 2 shows the energy dependence of the scintillator sensitivity in the form it is used in the data analysis.

C. Beamline attenuation

The beam line attenuation has been modeled with MCNP to get the fraction of the neutrons which hit the scintillator relative to those started at the TCC. An alternative model which computes the losses from the total interaction cross section of all materials in the beam line was also computed and found to be in good agreement with the MCNP output. The model included the port covers on the target chamber, the port and clean up collimator, the tungsten plate acting as a photon shield and the air between target chamber and detector. The resulting transmission factor as a function of neutron energy is shown in Fig. 3.

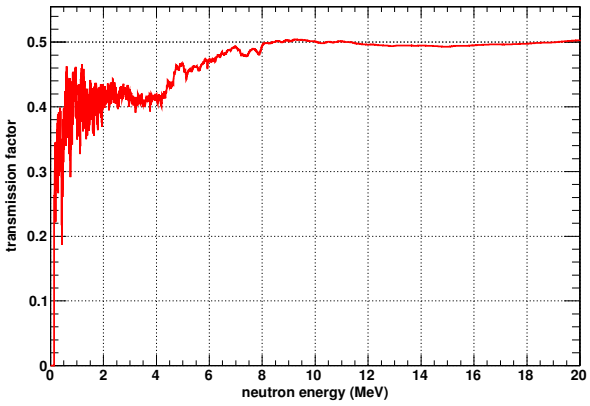

FIG. 3. The transmission factor from TCC to the detector as a function of neutron energy.

IV. MODEL OF THE NEUTRON SPECTRUM

The model used for the neutron spectrum, $I(E)$ in Eqn. (1), needs to be chosen such that the quantities of interest can be extracted from them. Two different approaches have been followed to model the spectrum: a physics independent form of a P-spline as described in Ref.[12] and a model based on a homogeneous plasma of a single temperature as described in Ref[13].

A. P-Spline fit of the data

Quantities like yield Y_n, DSR or $FWHM$ of the neutron spectrum can be extracted using the generic functional form of a spline. A spline is a piecewise polynomial function. Different polynomial pieces connect with each other at the so called knot points, where continuity and smoothness conditions are applied. Any spline function used as the model $I(E)$ can be expressed as a sum of

basis splines (B-Splines)

$$I(E) = \sum_i a_i B_{i,k}(E). \tag{4}$$

Here k indicates the order of polynomials used with $k = 4$ corresponding to cubic polynomials. Given a set of knots $t_0 = \ldots = t_k < \ldots < t_{n-k} = \ldots = t_n$ the B-Splines can be calculated recursively using

$$B_{i,1}(E) = \begin{cases} 1 & \text{if } t_i \leq E < t_{i+1} \\ 0 & \text{otherwise} \end{cases} \tag{5}$$

$$B_{i,k}(E) = \frac{E - t_i}{t_{i+k-1} - t_i} B_{i,k-1}(E) + \frac{t_{i+k} - E}{t_{i+k} - t_{i+1}} B_{i+1,k-1}(E).$$

One issue with these B-Splines is the choosing of the knots: if there are too many over a given region then the fitted curve will show more variation than the data justifies, whereas too few knots do not allow the curve to change fast enough to fit the data well. To overcome this problem the P-spline method[12] uses a dense set of knots and adds a penalty to the χ^2 enforcing a certain smoothness to the fit. The penalty term takes the form:

$$\lambda \sum_j (P_{ij} a_j)^2 = \lambda \|Pa\|_2^2 \tag{6}$$

with the penalty matrix P defined as:

$$P_{ij} = \begin{cases} (-1)^{j-i} \binom{k}{j-i} & \text{for } j - k \leq i \leq j \\ 0 & \text{otherwise} \end{cases} \tag{7}$$

The penalty magnitude λ is a positive number that needs to be chosen large enough to suppress oscillations of the solution but low enough to receive a good fit to the data. To choose the optimal λ the penalty term is plotted as function of the residual χ^2 on a log-log-plot for different values of λ; this plot is called the L-curve. The λ corresponding to the highest curvature of the L-curve is chosen for the best solution. Fig. 4 shows the P-spline fit and the resulting neutron spectrum, while Fig. 5 shows the L-curve for this fit, illustrating how the optimal value for λ is found.

Since the P-Spline is described in the neutron energy domain and has no characteristic energy associated with it, it is necessary to know the bang time as well as the detector timing to be able to determine t_0 of (1) in order to convert neutron time-of-flight into neutron energy. The bang time has to be taken from a different target diagnostic at NIF (e.g. SPIDER[14], GRH[15]) and the time-offset from the fiducial signal have to be determined from an timing shot, which utilizes a gold disk target that produces X-rays as soon as the Laser hits the target and can therefore be used to establish absolute timing. It is important to note that this spline fit is linear, i.e. the minimum of the χ^2 can be determined by a single matrix inversion.

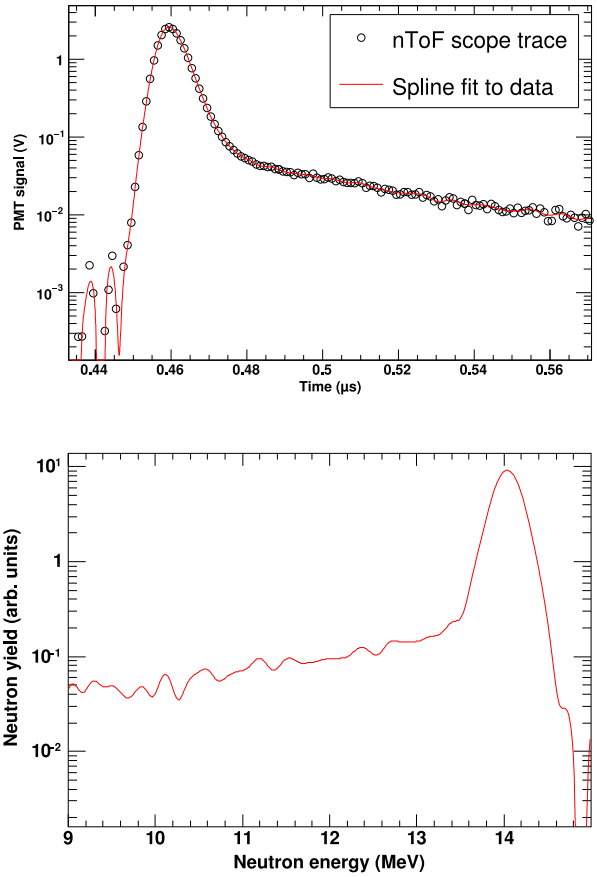

FIG. 4. P-Spline fit to the nToF data and the resulting neutron spectrum. DSR can be obtained by numerical integration of the spline function of the neutron spectrum from 10 to 12 MeV and dividing it by the integral from 13 to 15 MeV.

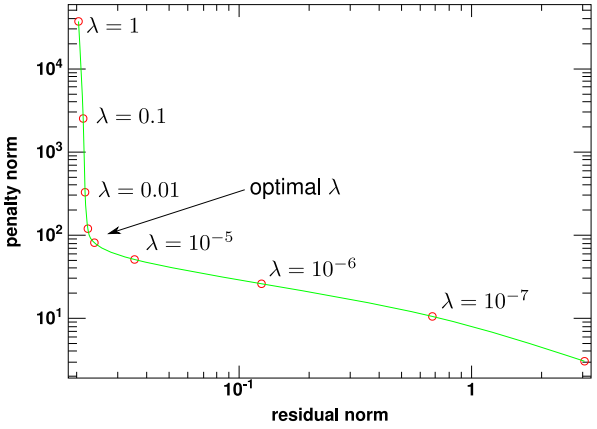

FIG. 5. L-curve for the P-Spline fit from Fig. 4

B. Physics model of a single temperature plasma with single scatter addition

To extract an ion temperature the birth spectrum can be modeled as a homogeneous and static, neutron emitting plasma at a single temperature[13,16]. The neutron energy of a fusion reaction at zero temperature can be calculated from the mass of neutron m_n, the mass of the product m_r and the Q-value as

$$E_0 = \frac{Q\,(Q/2 + m_r)}{Q + m_r + m_n}. \tag{8}$$

The distribution of the neutron energies assumed has the form:

$$I_{src}(E) = \frac{1}{\sqrt{2\pi\sigma^2}} \exp\left(-\frac{2\bar{E}}{\sigma^2}\left(\sqrt{E} - \sqrt{\bar{E}}\right)^2\right) \tag{9}$$

In this model the mean energy of the distribution and the second central moment are calculated from the T_{ion} of the plasma as:

$$\langle E\rangle = E_0 + \Delta E_{th} \tag{10}$$

and

$$\left\langle (E - \langle E\rangle)^2 \right\rangle = 4E_0 \frac{m_n}{m_n + m_r}\,(1 + \delta_w)\,T_{ion}. \tag{11}$$

Both ΔE_{th} and δ_w are calculated with the same expression

$$\frac{\alpha_1}{1 + \alpha_2 T_{ion}^{\alpha_3}} T_{ion}^{2/3} + \alpha_4 T_{ion}$$

where the values for $\alpha_1, \ldots, \alpha_4$ are taken from Table III in Ref[13].

This model uses a total of 3 parameters: the amplitude of the signal, the ion temperature and the time offset. For shots where there is significant scattering a model for the scattered spectrum has been added with a fourth parameter, which assumes a single down-scatter of a neutron. The shape of the scatter spectrum is computed as:

$$I_{scat}(E_f) = \int_{E_f}^{\infty} I_{src}(E_i) \frac{d\sigma}{d\Omega}(\cos\theta^{(CM)}) \frac{d\Omega}{dE_i} dE_i \tag{12}$$

where $\frac{d\sigma}{d\Omega}$ is the differential cross section and $\cos\theta^{(CM)}$ can be calculated from the initial and final energies of the scattered neutron:

$$\cos\theta^{(CM)} = \frac{(E_f^{(lab)} + m_n)E_t^{(CM)} - E_f^{(CM)} E_t^{(lab)}}{p_i^{(lab)} p_f^{(CM)}} \tag{13}$$

$$2E_f^{(CM)} E_t^{(CM)} = \left(E_t^{(CM)}\right)^2 + m_n^2 + m_R^2 \tag{14}$$

$$\left(E_t^{(CM)}\right)^2 = m_n^2 + m_S^2 + 2(E_i^{(lab)} + m_n)m_S \tag{15}$$

$$p_i^{(lab)} = \sqrt{E_i^{(lab)}(E_i^{(lab)} + 2m_n)} \tag{16}$$

$$p_f^{(CM)} = \sqrt{\left(E_f^{(CM)}\right)^2 - m_n^2} \tag{17}$$

with:

$E_i^{(lab)}$	initial neutron energy in lab system
$E_f^{(lab)}$	final neutron energy in lab system
$E_t^{(lab)}$	total energy in lab system ($E_i^{(lab)} + m_n + m_S$)
$E_f^{(CM)}$	final neutron energy in C.M. system
$E_t^{(CM)}$	total energy in C.M. system
$p_i^{(lab)}$	initial momentum in lab system
$p_f^{(CM)}$	final momentum in C.M. system
m_n	mass of neutron
m_S	mass of nucleus that is being scattered on
m_R	mass of recoiling nucleus (m_S+ excitation energy)

For the calculation of Eqn. (12) the differential cross sections of the elastic scattering of neutrons on tritium and deuterium have been fitted with a series of Legendre polynomials in $\cos\theta$:

$$\frac{d\sigma}{d\Omega}(\cos\theta) = \sum_{\ell=0}^{N} a_\ell P_\ell(\cos\theta) \tag{18}$$

For scattering on deuterium a fit with 9 coefficients ($a_0 \ldots a_8$) was chosen to parameterize the differential scattering cross section: 51.6 mb/sr, 52.5 mb/sr, 59.5 mb/sr, -17.4 mb/sr, 20.8 mb/sr, -14.8 mb/sr, 7.73 mb/sr, -4.92 mb/sr, 3.11 mb/sr. The differential scattering cross section on tritium needed only 5 coefficients: 79.2 mb/sr, 116 mb/sr, 118 mb/sr, 14.8 mb/sr, 14.8 mb/sr. The scattering model used assumed 50% deuterium and 50% tritium mixture as scattering source and the total neutron spectrum hitting the detector is then given as a linear combination of these:

$$I(E) = A\left(I_{src}(E) + \frac{1}{2} f_{scat}(I_{d\_scat}(E) + I_{t\_scat}(E))\right) \tag{19}$$

This gives the fit function a total of four parameters: a time offset t_0, an amplitude of the spectrum A, the ion temperature T_{ion} and scattering amplitude f_{scat}. It is important to point out that in this case the time offset can be obtained by the fit since the energy spectrum of the neutron is determined by the model.

V. DATA ANALYSIS

In the following section the application of the forward fitting method to actual shot data from the NIF will be examined in detail. The analysis of the nToF data depends on the type of shot being analyzed. For the DD

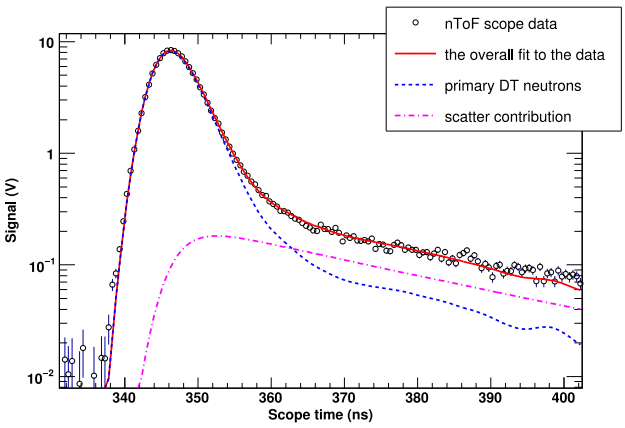

FIG. 6. Example of a fit to a DT time-of-flight neutron spectrum obtained from a NIF shot of the HiFoot series[18]. The fit uses the model described by Ballabio *et al.*[13] with the addition of a single scatter spectrum. Also shown are the unperturbed and the scatter component by itself.

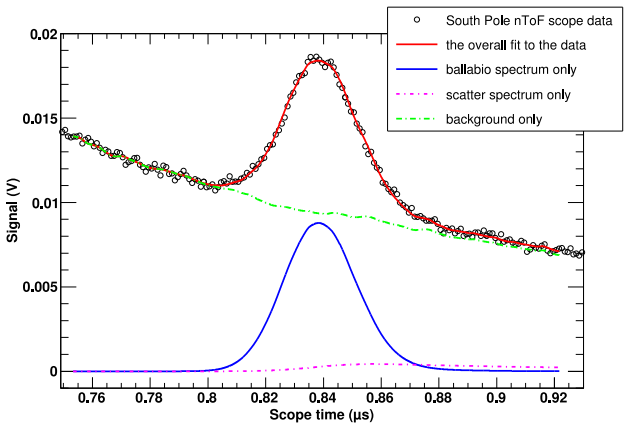

FIG. 7. Example of a fit to the DD peak in the time-of-flight neutron spectrum with the presence of the background from the DT peak, which shows the different contributions to the fit.

neutron peak on shots without tritium the ion temperature and neutron yield can be determined from a three parameter fit using Eqn (9). For high purity tritium shots the TT yield (experimentally defined as neutrons from 5 to 10 MeV) can be determined either using a spline fit or by using an R-matrix model of the TT neutron spectrum as described in Ref[17]. Shots with significant fraction of both tritium and deuterium show both DD and DT neutron peaks which can be fitted as described below.

A. Analysis of the primary DT fusion neutron peak

Fig. 6 shows an example fit of the model described by Eqns. (9)-(19). In this fit the ion temperature is extracted directly as a fit parameter whereas the primary neutron yield is obtained by numerical integration of the fit result from 13 to 15 MeV neutron energy. Likewise the DSR is calculated as the ratio of the two numerical integrations from 10 to 12 MeV and 13 to 15 MeV. The uncertainties of the individual data points are dominated by the scope noise which can be seen by the fact that the χ^2 per degree of freedom is typically between 1 and 1.4. To determine the primary neutron yield it is necessary to obtain a calibration constant in order to be able to convert the charge of the nToF detector into neutron yield. This constant was determined by calibrating against a neutron activation diagnostic[19] on an exploding pusher[20] shot. Since these shots have almost no compression the low areal density of the fuel ensures very little down scatter and therefore an isotropic neutron yield making them ideal for calibration purposes.

B. Analysis of DD peak

The peak of the DD neutrons on a DT shot can be recorded using a gated PMT. Fig. 7 shows the spectrum recorded by the gated PMT. The analysis of this data is complicated due to the fact that there are several more components to the signal. The individual components are: the neutrons from DD reactions, background from previously recorded signal due to the IRF of the detector, signal from lower energy neutrons such as down-scattered DT neutrons and neutrons from TT reactions as well as down-scattered DD neutrons.

By comparing the scope trace of a low ρR exploding pusher shot with that of a cryogenic layered shot it can be concluded that the background under the DD peak is dominated by neutron produced signal rather that scintillator decay from the gated off DT peak. The model for the fit has therefore an additional parabolic component to model the neutron induced background underneath the DD peak in the fit region from $E_n = 2 - 3$ MeV.

Due to the nature of this parabolic background it is not possible to determine the amount of down scattered DD neutrons directly from the fit. To include the scatter component an MCNP5 simulation of a capsule was constructed in order to determine the DD scattering contribution and yield correction as a function of DT DSR. A spherical burn spot of radius 25 μm were placed inside spherically concentric capsule with four regions:

- Low density DT hot spot ($T = T_{ion}$), $\rho = 20$ g/cm^3, $r < 25$ μm
- Low density DT cold plasma ($T = T_{rad}$), 25 μm $< r <$ 50 μm
- High density DT cold plasma ($T = T_{rad}$), 50 μm $< r <$ 60 μm

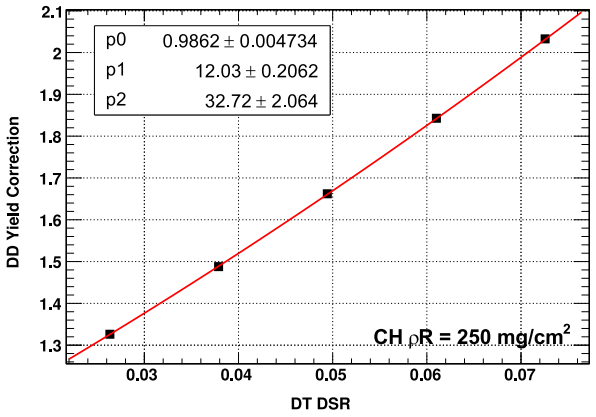

FIG. 8. MCNP model of the hotspot determining the ratio of total DD yield to unscattered DD yield for different DT DSR, which also assumes a CH ρR of 250 mg/cm^2 from remaining ablator mass. A parabolic fit has been used to interpolate between data points.

- High density CH cold plasma ($T = T_{rad}$), 60 μm $< r <$ 70 μm

where T_{ion} is the ion temperature, and T_{rad} is the radiation temperature inside the hohlraum (set to be 300 eV for all of these simulations). DT and DD source neutrons were generated using the Ballabio model and chosen to uniformly fill the inner hot spot sphere. The model was run for several values of T_{ion}, DT fuel and CH ablator densities. The model with areal density of the CH ablator equal to 250 mg/cm^2 was chosen to match the "typical" reported values of CH ρR from the GRH diagnostic in Hi-Foot experiments[21], and these simulations are the basis of the values plotted in Fig. 8.

It is important to note that the signal quality of the gated PMTs suffers due to the limitations of the gating system: the gate of the PMT needs considerable time to turn on and stabilize. This necessitates the use of high light attenuators in front of the PMT which increases considerably the noise in the signal due to limited photon statistics.

The fit shown in Fig. 7 allows the determination of DD T_{ion} and DD neutron yield, defined here as the signal coming from the DD peak and its down-scatter. The yield calibration is again obtained relative to a neutron activation diagnostic on an exploding pusher shot.

VI. UNCERTAINTIES OF DEDUCED VALUES

There are several different sources of uncertainty for the deduced values of Y_n, T_{ion} and DSR: statistical uncertainties due scope noise, neutron statistics and photo electron statistics as well as systematic uncertainties due to calibration, uncertainties in the IRF and the applied scatter model and the chosen fit range.

For the Y_n value the statistical uncertainties are below 1% whereas the calibration to the neutron activation diagnostics has a 7% uncertainty. Another part of the Y_n uncertainty are the light attenuators used. Currently the attenuation factor of identical designed light attenuator can vary by as much as 15%. Calibrations are planed for individual filters to lower this uncertainty to $\approx$ 5%. Therefore the dominating uncertainty for DT yield comes from systematics and is of the order of 9%.

The statistical uncertainties due to photo electrons are small compared to the scope noise, which gets included into the χ^2 of the fit. This changes the fit to have effectively equal weighting of all data points. Comparing fits to simulated data with either equal weighted uncertainties or Poisson error bars shows that the deduced T_{ion} can vary by about 150 eV. This systematic uncertainty is introduced due to the scope noise masking the actual Poisson uncertainty. Another systematic uncertainty comes due to the scatter model in the fit which assumes a single scatter from a thin shell of DT cold fuel. Comparing fit results from different simulations this uncertainty has been determined to be 50 eV. It has also been observed that the deduced T_{ion} result changes depending on the chosen range over which the fit minimizes the χ^2: the region for fitting the primary DT peak is from 5% of the peak height to the data point corresponding to $\approx$ 10 MeV neutron energy. The starting point was chosen to exclude any contributions from tertiary neutrons, while the end point is a good approximation to where the single scatter approximation remains valid. Changing the fit range has been observed to change the deduced T_{ion} by approximately 100 eV. The ion temperature depends on accuracy of the IRF shape. Since the ion temperature is defined through the second central moment in neutron energy space, but the IRF acts exclusively in the time domain and no direct relation to a single moment of IRF exists. To estimate the uncertainty introduced by the IRF the standard deviation $\sigma_{T_{ion}}$ for several different PMT (with each having its own IRF) recording the same neutron peak has been determined to be 150 eV. This part shows only statistical variations in the IRF due to construction, additional systematics of the IRF, such as for example systematically overestimating its width due to the finite width of the X-ray pulse used to construct it, are small and have been estimated to be 50 eV or less. The statistical uncertainty comes from the covariance matrix of the fit and is typically 50 eV. All errors have been added in quadrature and the result separated by statistical or systematical source are summarized in Table I.

The uncertainty of the DSR has three components: a systematical uncertainty due to the shape uncertainty of the IRF, an uncertainty due to the noise introduced in the IRF construction and the statistical uncertainty from the fit itself. The influence of the IRF shape has been tested by fitting exploding pusher shots where the down-scattered signal should be negligibly small and the uncertainty on the DSR value was determined to be 0.002–

TABLE I. Overview over uncertainties from nToF measurements. Relative uncertainties are given as percentage whereas absolute value are given as values with units (where appropriate).

Quantity		uncertainty	
	statistical	systematic	total
DT Y_n	$< 1\%$	9%	9%
DT T_{ion}	$\approx 1\%$	240 eV	250 eV
DSR	$\approx 5\%$	$\approx 5\%$ (rel) and 0.003 (abs)	$\approx 7\%$ (rel) and 0.003 (abs)
DD Y_n	$\approx 2\%$	10%	10%
DD T_{ion}	$\approx 2\%$	270 eV	290 eV

0.004 depending on the detector looked at. The statistical uncertainty due to the scope noise obtained from the fit is typically 5%. Since the IRF was created from scope data it has the same noise contribution of about 5%. These values are also summarized in Table I.

The error analysis of the obtained values for DD yield and T_{ion} on DT shots is also dominated by systematic effects: it has been observed that the deduced T_{ion} depends on the parametrization of the background shape and the chosen fitting range. Also a slight variation in the assumed scintillator sensitivity changes the value of the deduced DD T_{ion}. By comparing the results from different PMTs recording the same spectrum this uncertainty has been determined to be 250 eV. The fit range varies the T_{ion} by about 100 eV. The statistical uncertainty from the fit is about 100 eV.

The DD neutron yield, defined here as the signal coming from the DD peak and its down-scatter has the same uncertainty constrains as the DT yield, which is $\approx 7\%$ plus the uncertainty from the light attenuators used in front of the PMT. The fit uncertainty is about 2%.

VII. SUMMARY

In the analysis of nToF spectra we chose forward fitting of a spectrum model to the data obtained as the means to obtain consistent values for neutron yield, ion temperature and down-scattered ratio. The fit starts with a model of the spectrum in neutron energy space and incorporates corrections for detector sensitivity, the attenuation along the line-of-sight as well as the time response of the instrument. Two different models have been implemented: a generic spline fit which allows to extract neutron yield, FWHM of the neutron peak and DSR and a model of a single temperature plasma with single scatter addition allowing the determination of an ion temperature. The latter can also be used to deduce a DD ion temperature and yield on a DT shot, by fitting the model with a background addition to the spectrum recorded from a gated PMT. The overall uncertainties for these measurements are typically 9% for the DT neutron yield, 10% for the DD neutron yield, 250 eV for DT ion temperature and 290 eV for the DD ion temperature. The uncertainty for the DSR is 7% relative with an 0.003 absolute added in quadrature.

ACKNOWLEDGMENTS

This work was performed under the auspices of the U.S. Department of Energy by Lawrence Livermore National Laboratory under Contract DE-AC52-07NA27344.

[1] R. A. Lerche, L. W. Coleman, J. W. Houghton, D. R. Speck, and E. K. Storm, Appl. Phys. Lett. **31**, 645 (1977).
[2] B. A. Remington, R. A. Lerche, and M. D. Cable, Rev. Sci. Instrum. **61**, 3128 (1990).
[3] T. J. Murphy, R. A. Lerche, C. Bennett, and G. Howe, Rev. Sci. Instrum. **66**, 930 (1994).
[4] J. D. Lindl, L. J. Atherton, P. A. Amednt, S. Batha, P. Bell, R. L. Berger, R. Betti, D. L. Bleuel, T. R. Boehly, D. K. Bradley, D. G. Braun, D. A. Callahan, P. M. Celliers, C. J. Cerjan, D. S. Clark, G. W. Collins, R. C. Cook, E. L. Dewald, L. Divol, S. N. Dixit, E. Dzenitis, M. J. Edwards, J. E. Fair, R. J. Fortner, J. A. Frenje, V. Y. Glebov, S. H. Glenzer, G. Grim, S. W. Haan, A. V. Hamza, B. A. Hammel, D. R. Harding, S. P. Hatchett, C. A. Haynam, H. W. Herrmann, M. C. Herrmann, D. G. Hicks, D. E. Hinkel, D. D. Ho, N. Hoffman, H. Huang, N. Izumi, B. Jacoby, O. S. Jones, D. H. Kalantar, R. Kauffman, J. D. Kilkenny, R. K. Kirkwood, J. L. Kline, J. P. Knauer, J. A. Koch, B. J. Kozioziemski, G. A. Kyrala, K. L. Fortune, O. L. Landen, D. Larson, R. Lerche, S. L. Pape, R. London, B. J. MacGowan, A. J. MacKinnon, T. N. Malsbury, E. R. Mapoles, M. M. Marinak, P. W. McKenty, N. Meezan, D. D. Meyerhofer, P. Michel, J. Milovich, J. D. Moody, M. Moran, K. A. Moreno, E. I. Moses, D. H. Munro, A. Nikroo, R. E. Olson, T. Parham, R. W. Patterson, K. Peterson, R. Petrasso, S. M. Pollaine, J. E. Ralph, S. P. Regan, H. F. Robey, M. D. Rosen, R. Sacks, J. D. Salmonson, T. C. Sangster, S. M. Sepke, D. H. Schneider, M. B. Schneider, M. Shaw, B. K. Spears, P. T. Springer, C. Stoeckl, L. J. Suter, C. A. Thomas, R. Tommasini, R. P. Town, B. M. VanWonterghem, R. Vesey, S. V. Weber, P. J. Wegner, K. Widman, C. C. Widmayer, M. Wilke, H. L. Wilkens, E. A. Williams, D. C. Wilson, and B. K. Young, Nucl. Fusion **51**, 094024 (2011).
[5] M. J. Edwards, P. K. Patel, J. D. Lindl, L. J. Atherton, S. H. Glenzer, S. W. Haan, J. D. Kilkenny, O. L. Landen, E. I. Moses, A. Nikroo, R. Petrasso, T. C. Sangster, P. T. Springer, S. Batha, R. Benedetti, L. Bernstein, R. Betti, D. L. Bleuel, T. R. Boehly, D. K. Bradley, J. A. Caggiano, D. A. Callahan, P. M. Celliers, C. J. Cerjan, K. C. Chen, D. S. Clark, G. W. Collins, E. L. Dewald, L. Divol, S. Dixit, T. Doeppner, D. H. Edgell, J. E. Fair, M. Farrell, R. J. Fortner, J. Frenje, M. G. G. Johnson, E. Giraldez, V. Y. Glebov, G. Grim, B. A. Hammel, A. V. Hamza, D. R. Harding, S. P. Hatchett, N. Hein, H. W. Herrmann, D. Hicks, D. E. Hinkel, M. Hoppe, W. W. Hsing, N. Izumi, B. Jacoby, O. S. Jones, D. Kalantar, R. Kauffman, J. L. Kline, J. P. Knauer, J. A. Koch, B. J. Kozioziemski, G. Kyrala, K. N. LaFortune, S. L. Pape, R. J. Leeper, R. Lerche, T. Ma, B. J. MacGowan, A. J. MacKinnon, A. Macphee, E. R. Mapoles, M. M. Marinak, M. Mauldin, P. W. McKenty, M. Meezan, P. A. Michel, J. Milovich, J. D. Moody, M. Moran, D. H. Munro, C. L. Olson, K. Opachich, A. E. Pak, T. Parham, H.-S. Park, J. E. Ralph, S. P. Regan, B. Remington, H. Rinderknecht, H. F. Robey, M. Rosen, S. Ross, J. D. Salmonson, J. Sater, D. H. Schneider, F. H. Séguin, S. M. Sepke, D. A. Shaughnessy, V. A. Smalyuk, B. K. Spears, C. Stoeckl, W. Stoeffl, L. Suter, C. A. Thomas, R. Tommasini, R. P. Town, S. V. Weber, P. J. Wegner, K. Widman, M. Wilke, D. C. Wilson, C. B. Yeamans, and A. Zylstra, Phys. Plasmas **20**, 070501 (2013).

[6]T. J. Clancy, J. Caggiano, J. McNaney, M. Eckart, M. Moran, V. Y. Glebov, J. Knauer, R. Hatarik, S. Friedrich, R. Zacharias, A. Carpenter, M. J. Shoup, T. Buczek, M. Yeoman, Z. Zeid, N. Zaitseva, B. Talison, J. Worden, B. Rice, T. Duffy, A. Pruyne, and K. Marshall, Proc. of SPIE **9211**, 92110A (2014).

[7]R. Hatarik, J. A. Caggiano, V. Glebov, J. McNaney, C. Stoeckl, and D. H. G. Schneider, Plasma and Fussion Research **9**, 4404104 (2014).

[8]V. Y. Glebov, C. Forrest, J. P. Knauer, A. Pruyne, M. Romanofsky, T. C. Sangster, M. J. S. III, C. Stoeckl, J. A. Caggiano, M. L. Carman, T. Clancy, R. Hatarik, J. McNaney, and N. P. Zaitzeva, Rev. Sci. Instrum. **83**, 10D309 (2012).

[9]G. P. Grim, G. L. Morgan, R. Aragonez, T. N. Archuleta, D. E. Bower, C. R. Danly, O. B. Drury, J. M. Dzenitis, V. E. Fatherley, B. Felker, D. N. Fittinghoff, N. Guler, F. E. Merrill, J. A. Oertel, C. H. Wilde, and M. D. Wilke, Proc. of SPIE **8854**, 88540G (2013).

[10]N. R. Stanton, "A monte carlo program for calculating neutron detection efficiencies in plastic scintilator," Tech. Rep. COO-1545-92 (University of Colorado, Boulder, 1971).

[11]V. V. Verbinski, W. R. Burrus, T. A. Love, W. Zobel, and N. W. Hill, Nucl. Inst. and Meth. **65**, 8 (1968).

[12]P. H. C. Eilers and B. D. Marx, Statist. Sci. **11**, 89 (1996).

[13]L. Ballabio, J. Källne, and G. Gorini, Nucl. Fusion **38**, 1723 (1998).

[14]S. F. Khan, P. M. Bell, D. K. Bradley, S. R. Burns, J. R. Celeste, L. S. Dauffy, M. J. Eckart, M. A. Gerhard, C. Hagmann, D. I. Headley, J. P. Holder, N. Izumi, M. C. Jones, J. W. Kellogg, H. Khater, J. R. Kimbrough, A. G. MacPhee, Y. P. Opachich, N. E. Palmer, R. B. Petre, J. L. Porter, R. Shelton, T. L. Thomas, and J. B. Worden, Proc. of SPIE **8505**, 850505 (2012).

[15]H. W. Herrmann, N. Hoffman, D. C. Wilson, W. Stoeffl, L. Dauffy, Y. H. Kim, A. McEvoy, C. S. Young, J. M. Mack, C. J. Horsfield, M. Rubery, E. K. Miller, and Z. A. Ali, Rev. Sci. Instrum. **81**, 10D333 (2010).

[16]H. Brysk, Plasma Phys. **15**, 611 (1973).

[17]D. B. Sayre, C. R. Brune, J. A. Caggiano, V. Y. Glebov, R. Hatarik, A. D. Bacher, D. L. Bleuel, D. T. Casey, C. J. Cerjan, M. J. Eckart, R. J. Fortner, J. A. Frenje, S. Friedrich, M. Gatu-Johnson, G. P. Grim, C. Hagmann, J. P. Knauer, J. L. Kline, D. P. McNabb, J. M. McNaney, J. M. Mintz, M. J. Moran, A. Nikroo, T. Phillips, J. E. Pino, B. A. Remington, D. P. Rowley, D. H. Schneider, V. A. Smalyuk, W. Stoeffl, R. E. Tipton, S. V. Weber, and C. B. Yeamans, Phys. Rev. Lett. **111**, 052501 (2013).

[18]O. A. Hurricane, D. A. Callahan, D. T. Casey, E. L. Dewald, T. R. Dittrich, T. Döppner, M. A. B. Garcia, D. E. Hinkel, L. F. B. Hopkins, P. Kervin, J. L. Kline, S. L. Pape, T. Ma, A. G. MacPhee, J. L. Milovich, J. Moody, A. E. Pak, P. K. Patel, H.-S. Park, B. A. Remington, H. F. Robey, J. D. Salmonson, P. T. Springer, R. Tommasini, L. R. Benedetti, J. A. Caggiano, P. Celliers, C. Cerjan, R. Dylla-Spears, D. Edgell, M. J. Edwards, D. Fittinghoff, G. P. Grim, N. Guler, N. Izumi, J. A. Frenje, M. G. Johnson, S. Haan, R. Hatarik, H. Herrmann, S. Khan, J. Knauer, B. J. Kozioziemski, A. L. Kritcher, G. Kyrala, S. A. Maclaren, F. E. Merrill, P. Michel, J. Ralph, J. S. Ross, J. R. Rygg, M. B. Schneider, B. K. Spears, K. Widmann, and C. B. Yeamans, Phys. Plasmas **21**, 056314 (2014).

[19]C. B. Yeamans, D. L. Bleuel, and L. A. Bernstein, Rev. Sci. Instrum. **83**, 10D315 (2012).

[20]M. Gatu-Johnson, D. T. Casey, J. A. Frenje, C.-K. Li, F. H. Séguin, R. D. Petrasso, R. Ashabranner, R. Bionta, S. LePape, M. McKernan, A. Mackinnon, J. D. Kilkenny, J. Knauer, and T. C. Sangster, Phys. Plasmas **20**, 042707 (2013).

[21]O. A. Hurricane, D. A. Callahan, D. T. Casey, P. M. Celliers, C. Cerjan, E. L. Dewald, T. R. Dittrich, T. Dppner, D. E. Hinkel, L. F. B. Hopkins, J. L. Kline, S. L. Pape, T. Ma, A. G. MacPhee, J. L. Milovich, A. Pak, H.-S. Park, P. K. Patel, B. A. Remington, J. D. Salmonson, P. T. Springer, and R. Tommasini, Nature **506**, 343 (2014).